Synthesis and Characterization of Regioregular Polymers Containing Substituted Thienylene/Bithienylene and Phenylene Repeating Units

S. C. Ng,[†] J. M. Xu, and Hardy S. O. Chan*,[†,‡]

Departments of Chemistry and Materials Science, National University of Singapore, Kent Ridge, Singapore 119260

Received November 30, 1999; Revised Manuscript Received July 11, 2000

ABSTRACT: Regioregular polymers poly(3-alkyl-2,5-thienylene-*alt*-1,4-phenylene) (PBTC$_n$, $n = 4, 8, 12$) and poly[1,4-bis(3-alkyl-2-thienyl)phenylene] (PBTBC$_n$, $n = 4, 8, 12$), which contain alternating phenylene and substituted thienylene or bithienylene repeating units, have been chemically and/or electrochemically synthesized and characterized. Their structures are consistent with that expected as indicated by NMR, FTIR, and microanalysis. The change in glass transition temperature and UV−vis and fluorescence spectra with modification of polymer backbone and increase of the alkyl chain length has been observed and discussed. The PBTC$_n$ series shows better thermal stability in air, and the compounds in the series are partially crystalline. The PBTC$_n$ polymers have liquid crystalline properties as shown by MDSC, XRD, and polarized optical microscopy. XPS study performed on both the neutral and doped states shows the formation of charge carrier in the polymer backbone when doped. The polymers are both p- and n-dopable as indicated by cyclic voltammetry. Electrochromism when the polymers are p-doped is also evidenced by the spectral changes in UV−vis−NIR region.

Introduction

Functionalized polythiophenes and polybithiophenes are interesting mterials due to their processability and property tunability attained upon functionalization. Regioregular copolymers consisting of alternating thiophene and aromatic units (see Chart 1A) have also been

Chart 1. Polymer Structure

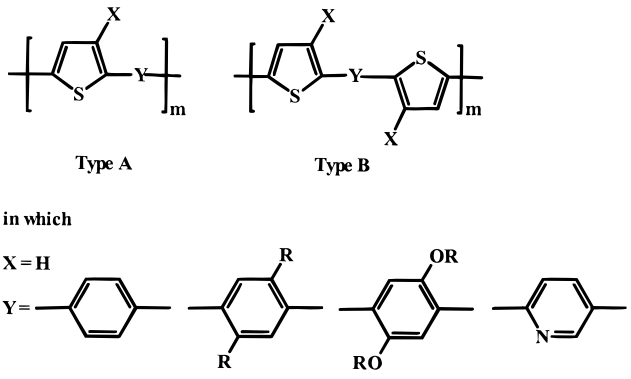

reported extensively in recent years. They are usually synthesized via organometallic polycondensation methods, such as Stille coupling,[1,2] Suzuki coupling,[3,4] Nigishi coupling,[5,6] zerovalent nickel complex catalyzed polycondensation using halogen substituted aromatics as starting materials[7,8] and Grignard coupling.[9] Most of these polymers have been reported to be fluorescent,[1,2,4,6,8,9] electroactive,[3,5−9] and crystalline[1,3,7] and exhibit nonlinear optical properties[8] due to their rigid backbone structure. Polymer LEDs, based on structures similar to that of type A,[2,4,8] have received special attention recently as they have shown great commercial potential.

Another family of copolymers containing bithiophene or substituted bithiophene (see Chart 1B) can be polymerized chemically by $FeCl_3$ or electrochemically[6,10−12] because of the very high reactivity at the α site of the thiophene ring in the monomer. As type A and type B are structurally similar, it would be interesting to make a systematic and comparative study between these two types of polymers. In this work, we report in detail the synthesis and characterization of a series of type A and type B polymers (see structure 2) using fluorescence spectrometry, UV−vis absorption spectrometry, modulated differential scanning calorimetry (MDSC), thermogravimetry (TG), X-ray diffraction (XRD), X-ray photoelectron spectroscopy (XPS), and cyclic voltammetry (CV). Some of the preliminary results obtained in this research program have already been reported earlier[9,13] but some of the data will be used here for comparative purposes where appropriate.

Experimental Section

Materials. Diethyl ether (J. T. Baker, A. R.) was dried over sodium coils. THF (J. T. Baker, A. R.) was freshly distilled from sodium coil and benzophene. Chloroform (J. T. Baker, A. R.) was first washed with water to remove alcohol, dried and distilled from P_2O_5. Nitromethane (Fisher, A. R.) was distilled from CaH_2 and stored over 4 Å molecular sieve. Acetonitrile (Reagent Chemicals, A. R.) was freshly distilled from CaH_2.

Anhydrous ferric chloride (Riedel-deHaen, 99%), *N*-bromosuccinimide (Merck, 99%), 3-bromothiophene (Fluka, >95%), 1-bromobutane (Merck, 98%), 1-bromohexane (Merck, 98%), 1-bromododecane (Merck, 97%), Ni(dppp)Cl_2 (Fluka, >95%), butyllithium (TCI, 15% in hexane), magnesium (Fluka, 99.8%), 1,2-dibromoethane (BDH, 99%), hydrazine hydrate (Fluka, 99.0%), and iodine for synthesis (Fisher, >99%) were used as received. Bu_4NBF_4 (TCI, for electrochemistry) was dried under high vacuum at 60 °C for 24 h prior to use. 3-Butylthiophene, 3-octylthiophene, 3-dodecylthiophene, 3-butyl-2-bromothiophene, 3-octyl-2-bromothiophene, and 3-dodecyl-2-bromothiophene were synthesized as reported by McCullough et al.[14]

Instrumentation. ^{1}H NMR spectra were recorded on a 300 MHz Bruker ACF 300 FT-NMR spectrophotometer. ^{13}C NMR

* Corresponding author.
[†] Department of Chemistry, National University of Singapore.
[‡] Department of Materials Science, National University of Singapore.

10.1021/ma992000t CCC: $19.00
Published on Web 09/13/2000

Scheme 1. Synthetic Route to the Monomers and Polymers[a]

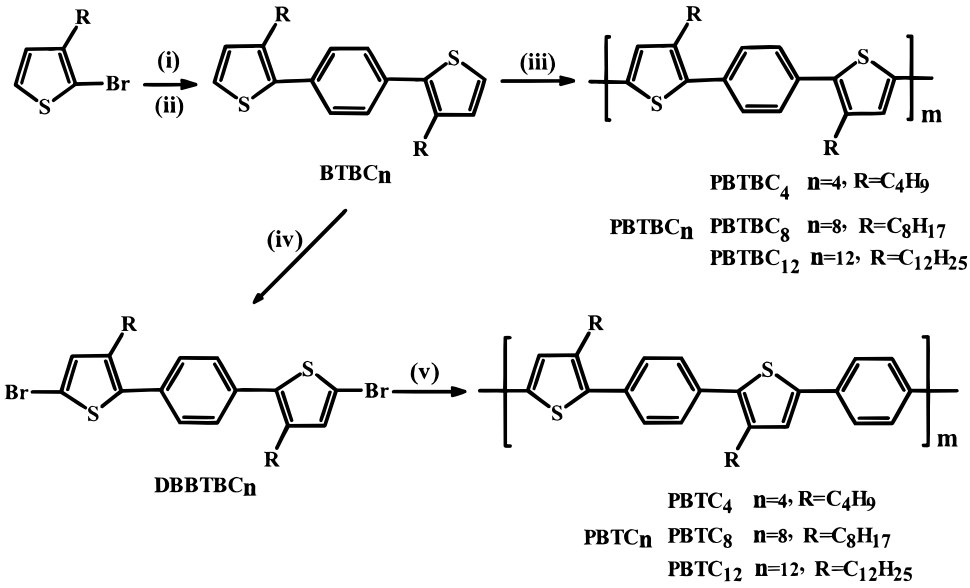

[a] Reagents and Conditions: (i) Mg, Et_2O; (ii) 1,4-dibromobenzene, Ni(dppp)Cl_2; (iii) 4 equiv of $FeCl_3$, $CHCl_3$; (iv) 2 equiv of Br_2, Acoh/$CHCl_3$; (v) (a) *n*-BuLi, THF; (b) $MgBr_2 \cdot Et_2O$; (c) 1,4-dibromobenzene, Ni(dppp)Cl_2, THF.

(62.9 MHz) spectra were obtained using the same instrument. Deuterated chloroform was used as solvent and tetramethylsilane (TMS) as the internal reference. EIMS spectra were obtained using a micromass 7034E mass spectrometer. HRMS spectra were obtained using either E-SCAN or peak match method. Elemental analyses of all the monomers and polymers were conducted at the NUS Microanalytical Laboratory on a Perkin-Elmer 240C elemental analyzer for C, H, and S determination. Halogen determinations were done either by ion chromatography or the oxygen flask method. Gel permeation chromatography (GPC) analyses were carried out using a Perkin-Elmer model 200 HPLC system with Phenogel MXL and MXM columns (300 mm × 4.6 mm ID, MW 100−100K and 5K-500K, respectively) calibrated using polystyrene standards. THF was used as eluant, and the flow rate was 0.35 mL min^{-1}. FTIR spectrum of the polymer dispersed in KBr disks was recorded on a Bio-Red TFS 156 spectrometer. Solution phase absorption and fluorescence spectrum measurements were conducted on a Hewlett Parkard 8452A spectrophotometer and Shimadzu RF5000 fluorescence spectrophotometer, respectively. Dilute polymer solutions dissolved in spectro-grade chloroform (10^{-5}−10^{-6} M) were used for analysis. Optical absorption from thin polymer film deposited onto indium tin oxide (ITO) coated glass plate was obtained on a Lamda 900 spectrophotometer. Thermogravimetry (TG) was conducted on a Du Pont Thermal Analyst 2100 system with a TGA 2950 thermogravimetric analyzer in air or nitrogen (75 mL min^{-1}) at a heating rate of 10 °C from room temperature to 1000 °C. Modulated differential scanning calorimetry (MDSC) were conducted on a TA Instruments 2910 differential scanning calorimeter upgraded with a MDSC option in N_2 (70 mL min^{-1}) using a heating rate of 1 or 2 °C min^{-1}, an oscillation amplitude of 1 or 2 °C, respectively, and an oscillation period of 60 or 80 s from −100 to +170 °C unless otherwise stated. Conductivity measurements were carried out on polymer pellets of known thickness using a four-point probe connected to a Keithley constant current source. X-ray diffraction (XRD) pattern was obtained in reflection mode on a Siemens D-5005 wide-angle X-ray diffractometer with a Cu Kα light source. XPS measurement of polymer powder or films (on ITO) was performed by means of a VG ESCA/SIMLAB MKII with a Mg Kα radiation source (1253.6 eV). The binding energies were corrected for surface charging by referencing to the designated hydrocarbon C(1s) binding energy as 284.6 eV. Spectrum deconvolutions were carried out using the Gaussian component with the same full width at half-maximum (fwhm) for each component in a particular spectrum. Surface elemental stoichiometries were obtained from peak area ratios corrected with the appropriate experimentally determined sensitivity factors. Morphology of polymer films cast from solution or electrochemically produced were investigated on a Philips XL30-FEG scanning electromicroscopy (SEM) operated in the secondary electron mode in a vacuum chamber of 10^{-4} mbar. The presence of elements was determined using an energy-dispersive X-ray (EDX) spectrometer (Kevex Superquantum) attached to the microscope. Polarized optical microscopy of solution cast films was performed with a Leica DMLP microscope equipped with a Leica hot stage.

Electrochemical polymerization was achieved using an EG&G 273A potentiostat/galvanostat controlled by EG&G M270 research electrochemistry software and a three-electrode single compartment chemical cell consisted of an ITO glass plate as the working-electrode, a platinum wire as the counter electrode and a Ag/$AgNO_3$ (in 0.1 M acetonitrile) as the quasi-reference electrode [0.35 V vs saturated calomel electrode (SCE)]. Cyclic voltammetry of polymer films formed either by solution casting or electrochemically was carried out in a solution of 1 M Bu_4NBF_4 in acetonitrile under argon atmosphere. In situ electrochromism studies of polymers were conducted in a single-compartment, three electrode quartz cell comprising a film-coated ITO working-electrode, a platinum counter electrode, and a silver wire quasi-reference electrode using the potentiostat together with a Lamda 900 UV−Vis−NIR spectrometer in the same electrolyte system as CV.

Synthesis. Chemical Synthesis. The general schematic synthesis route is shown in Scheme 1. The structures of monomers and polymers were mainly verified by FTIR, ^{1}H NMR, and ^{13}C NMR spectra, as listed in Tables 1−3, respectively.

1,4-Bis(3-butyl-2-thienyl)benzene (BTBC$_4$). Magnesium (0.63 g, 26 mmol) and a few crystals of catalytic iodine were placed in an oven-dried, 100 mL two-neck round-bottom flask equipped with a magnetic stirrer and a condenser capped with a rubber septum. 2-Bromo-3-butylthiophene (5.47 g, 25.0 mmol) dissolved in ether (50 mL) was transferred into the flask under nitrogen atmosphere. Thereafter, the reaction mixture was refluxed for 2 h to afford a pale-colored Grignard reagent. This intermediate product was then transferred using a cannula into a 100 mL two-neck flask containing 1,4-dibromobenzene (2.36 g, 10.0 mmol) and Ni(dppp)Cl_2 (0.054 g, 0.10 mmol) in an ice bath. The solution was warmed to 35 °C and stirred for 48 h under nitrogen. The cooled reaction mixture was poured into 4 M aqueous HCl, and the aqueous layer was extracted with CH_2Cl_2. The combined organic layers were neutralized with water and dried over calcium chloride, and

Table 1. FTIR Absorptions (cm^{-1}) and Identities for the Monomers and Neutral Polymers

	arom C−H str				ring str			arom OOP bends	
compound	α	β	ϕ	aliphatic C−H str	phenylene	thiophene	CH_3 deform	phenylene	thiophene
$BTBC_4$[a]	3098	3059	3023	2953, 2926, 2857	1551	1468, 1433	1377	873	835, 725
$BTBC_8$[a]	3104	3065	3021	2953, 2924, 2855	1555	1466, 1437	1377	875	839, 721
$BTBC_{12}$[a]	3100	3057	3019	2953, 2919, 2851	1543	1466, 1437	1375	877	837, 731
$DBBTBC_4$[a]	3075	3050	3021	2957, 2926, 2864	1555	1499, 1468, 1439	1377	873	835, 727
$DBBTBC_8$[a]	3071	3044	3021	2955, 2924, 2853	1555	1504, 1466, 1437	1377	870	835, 721
$DBBTBC_{12}$[a]	3077	3046	3021	2957, 2922, 2851	1550	1500, 1466, 1441	1375	870	833, 721
$PBTBC_4$		3054	3023	2953, 2924, 2857	1603, 1543	1499, 1460, 1439	1377	873	831, 727
$PBTBC_8$		3052	3025	2953, 2922, 2851	1605, 1545	1499, 1460, 1441	1375	873	829, 721
$PBTBC_{12}$		3054	3025	2953, 2922, 2851	1605, 1545	1499, 1462, 1441	1375	873	831, 721
$PBTC_4$		3057	3023	2953, 2926, 2859	1562, 1545	1499, 1460, 1441	1377	873	830, 727
$PBTC_8$		3063	3025	2953, 2924, 2853	1653, 1543	1497, 1458, 1439	1373	877	829, 721
$PBTC_{12}$		3063	3025	2955, 2922, 2851	1653, 1545	1506, 1458, 1437	1375	873	835, 719

[a] The monomers also have peaks at around 1600 cm^{-1} ascribed to phenylene ring stretching, but they are very weak and are not reported here.

Table 2. ^1H NMR Resonances (ppm) and Identities for the Monomers and Neutral Polymers

compound	H-α	H-α_{end}	H-β	H-β_{end}	H-ϕ	H-ϕ_{end}	H−R
$BTBC_4$	7.23 (d)		6.99 (d)		7.47 (s)		2.71 (t), 1.63 (m), 1.35 (m), 0.90 (t)
$BTBC_8$	7.24 (d)		7.00 (d)		7.46 (s)		2.69 (t), 1.63 (m), 1.25 (m). 0.86 (t)
$BTBC_{12}$	7.24 (d)		6.99 (d)		7.46 (s)		2.69 (t), 1.63 (m), 1.25 (m). 0.88 (t)
$DBBTBC_4$			6.94 (s)		7.39 (s)		2.62 (t), 1.58 (m), 1.33 (m), 0.89 (t)
$DBBTBC_8$			6.94 (s)		7.38 (s)		2.60 (t), 1.58 (m), 1.25 (m), 0.86 (t)
$DBBTBC_{12}$			6.94 (s)		7.39 (s)		2.61 (t), 1.58 (m), 1.25 (m), 0.88 (t)
$PBTBC_4$		7.24 (d)	7.10 (m)	7.00 (d)	7.50 (m)		2.71 (m), 1.67 (m), 1.38 (m), 0.86 (m)
$PBTBC_8$		7.24 (d)	7.10 (m)	7.00 (d)	7.50 (m)		2.70 (m), 1.66 (m), 1.27 (m), 0.87 (m)
$PBTBC_{12}$		7.24 (d)	7.09 (m)	6.99 (d)	7.50 (m)		2.70 (m), 1.66 (m), 1.26 (m), 0.87 (m)
$PBTC_4$		7.23 (d)	7.10 (m)	7.00 (d)	7.50 (m)	7.64 (s)	2.73 (m), 1.67 (m), 1.40 (m), 0.94 (m)
$PBTC_8$		7.23 (d)	7.10 (m)	7.01 (d)	7.51 (m)	7.65 (s)	2.72 (m), 1.69 (m), 1.29 (m), 0.89 (m)
$PBTC_{12}$		7.23 (d)	7.09 (m)	7.00 (d)	7.50 (m)	7.64 (s)	2.70 (m), 1.57 (m), 1.25 (m), 0.86 (m)

Table 3. ^{13}C NMR Resonances (ppm) and Identities for the Monomers and Neutral Polymers

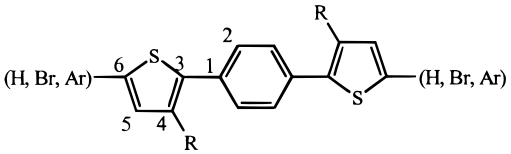

compound	C-1	C-2	C-3	C-4	C-5	C-6	C−R
$BTBC_4$	138.72	129.21	133.65	137.25	129.52	123.63	33.08, 28.35, 22.47, 13.78
$BTBC_8$	138.77	129.25	133.72	137.30	129.56	123.68	31.83, 30.96, 29.46, 29.35, 29.20, 28.69, 22.63, 14.05
$BTBC_{12}$	138.75	129.19	133.65	137.23	129.52	123.62	31.82, 30.91, 29.59, 29.55, 29.48, 29.40, 29.34, 29.25, 28.63, 22.58, 14.00
$DBBTBC_4$	139.51	129.20	132.97	138.62	132.19	110.49	32.87, 28.24, 22.34, 13.73
$DBBTBC_8$	139.55	129.19	132.98	138.61	132.18	110.48	31.72, 30.68, 29.23, 29.07, 28.52, 22.52, 13.95
$DBBTBC_{12}$	139.54	129.19	132.97	138.60	132.19	110.49	31.82, 30.70, 29.57, 29.54, 29.43, 29.24, 28.52, 22.58, 14.00
$PBTBC_4$	139.68	129.05	129.29	136.11	126.06	135.51	32.98, 28.58, 22.52, 13.83
$PBTBC_8$	139.72	129.04	129.28	136.08	126.06	135.51	31.76, 30.78, 29.40, 29,28, 29.13, 28.85, 22.55, 13.99
$PBTBC_{12}$	*a*	129.18	*a*	*a*	*a*	*a*	31.94, 31.27, 30.91, 29.67, 29.64, 29.54, 29.46, 29,38, 28.96, 22.71, 14.13
$PBTC_4$	139.67	129.05	131.85	135.51	126.06	133.36	32.98, 28.58, 22.57, 13.82
$PBTC_8$	139.72	129.05	131.86	135.53	125.75	133.26	31.79, 30.80, 29.43, 29.31, 29.17, 28.88, 22.59, 14.02
$PBTC_{12}$	139.72	129.03	129.27	135.53	126.04	133.36	31.82, 30.78, 29.56, 29.40, 29.33, 29.25, 28.85, 22.58, 14.00

[a] The solubility of $PBTBC_{12}$ is too low for the resonances to be well resolved.

the solvent was evaporated off. Double recrystallization from ethanol yielded a milk-colored needle-form product (1.98 g, 56% yield, mp 64−65 °C). EIMS *m/z* (relative intensity): 354 (M^+, 100), 311 ($M^+ - C_3H_7$, 28), 254 ($M^+-C_3H_7-C_4H_9$, 12%). HRMS: calculated for $C_{22}H_{26}S_2$ (M^+), 354.1476; found, 354.1487. Anal. Calcd for $C_{22}H_{26}S_2$: C, 74.58; H, 7.34; S, 18.08. Found: C, 73.98; H, 7.95; S, 17.86.

1,4-Bis(5-bromo-3-butyl-2-thienyl)benzene ($DBBTBC_4$). Bromine (1.88 g, 11.8 mmol) diluted in an AcOH/$CHCl_3$ (40 mL) mixture was added dropwise to a solution of $BTBC_4$ (1.98 g, 5.59 mmol) dissolved in $CHCl_3$ (20 mL) in a 100 mL two-neck flask at room temperature. The mixture was stirred for 24 h and extracted with $CHCl_3$, washed by large quantities of water, aqueous sodium carbonate, and water. The organic layer was dried over calcium chloride and the solvent removed. The product was obtained as a lemon-colored thick oil which then solidified at room temperature following silica gel column chromatography with hexane as eluant (2.71 g, 94% yield, mp 51−52 °C). EIMS *m/z* (relative intensity): 514 (M^++4, 61), 512 (M^+ + 2, 76), 510 (M^+, 58), 43 ($C_3H_7^+$, 100%). HRMS: calculated for $C_{22}H_{24}S_2Br_2$ ($M^+ + 2$), 511.9667; found, 511.9691. Anal. Calcd for $C_{22}H_{24}S_2Br_2$: C, 51.56; H, 4.69; S, 12.50; Br, 31.25. Found: C, 52.11; H, 5.04; S, 12.48; Br, 30.06.

1,4-Bis(3-octyl-2-thienyl)benzene ($BTBC_8$). $BTBC_8$ was synthesized in the same way as $BTBC_4$. The product was purified by double flash chromatography (hexane as eluant) as yellow oil (75% yield) that solidified at room temperature (mp 33−34 °C). EIMS *m/z* (relative intensity): 466 (M^+, 100), 367 ($M^+ - C_7H_{15}$, 36), 43 ($C_3H_7^+$, 58%). HRMS: calculated for $C_{30}H_{42}S_2$ (M^+), 466.2728; found, 466.2750. Anal. Calcd for $C_{30}H_{42}S_2$: C, 77.25; H, 9.01; S, 13.73. Found: C, 77.33; H, 8.68; S, 13.29.

1,4-Bis(5-bromo-3-octyl-2-thienyl)benzene (DBBTBC$_8$). BTBC$_8$ was brominated in the same way as BTBC$_4$ to afford DBBTBC$_8$ as a pale yellow liquid, which was purified by flash chromatography on silica gel using hexane as eluant (92% yield). EIMS *m*/*z* (relative intensity): 626 ($M^+ + 4$, 90), 624 ($M^+ + 2$, 100), 622 (M^+, 91), 43 ($C_3H_7^+$, 87%). HRMS: calculated for $C_{30}H_{40}S_2Br_2$ ($M^+ + 2$), 624.0981; found, 624.0942. Anal. Calcd for $C_{30}H_{40}S_2Br_2$: C, 57.69; H, 6.41; S, 10.26; Br, 25.46. Found: C, 56.16; H, 7.12; S, 9.85; Br, 26.82.

1,4-Bis(3-dodecyl-2-thienyl)benzene (BTBC$_{12}$). BTBC$_{12}$ was synthesized in the same way as BTBC$_8$ and isolated as an orange yellow oil (60% yield) that solidified at room temperature (mp 48−49 °C). EIMS *m*/*z* (relative intensity): 578 (M^+, 100), 423 ($M^+ - C_{11}H_{23}$, 15), 43 ($C_3H_7^+$, 43%). HRMS: calculated for $C_{38}H_{56}S_2$ (M^+), 578.3980; found, 578.3966. Anal. Calcd for $C_{38}H_{56}S_2$: C, 78.81; H, 10.03; S, 11.07. Found: C, 79.48; H, 10.70; S, 10.70.

1,4-Bis(5-bromo-3-dodecyl-2-thienyl)benzene (DBBTBC$_{12}$). BTBC$_{12}$ was brominated in the same way as BTBC$_4$ to afford DBBTBC$_{12}$ as a pale yellow solid (95% yield, mp 57−58 °C). EIMS *m*/*z* (relative intensity): 738 ($M^+ + 4$, 75), 736 ($M^+ + 2$, 100), 734 (M^+, 70), 43 ($C_3H_7^+$, 85%). HRMS: calculated for $C_{38}H_{56}S_2Br_2$ ($M^+ + 2$), 736.2192; found, 736.2224. Anal. Calcd for $C_{38}H_{54}S_2Br_2$: C, 61.96; H, 7.61; S, 8.70; Br, 21.74. Found: C, 61.79; H, 9.40; S, 8.32; Br, 22.72.

Poly[1,4-bis(3-butyl-2-thienyl)phenylene] (PBTBC$_4$). BTBC$_4$ (0.60 g, 1.7 mmol) was dissolved in dry $CHCl_3$ (8 mL) in a 50 mL round-bottom flask equipped with a stir bar and a N_2 inlet followed by addition of a slurry of $FeCl_3$ (1.11 g, 6.83 mmol) in $CHCl_3$ (27 mL). The mixture was stirred in an ice bath for 4 h and then at room temperature for 20 h. The mixture was poured into methanol to terminate the reaction, and then the product was filtered. The yellow solid obtained was extracted with methanol in a Soxhlet extractor (24 h) and then with acetone (4 h) in turn. The polymer was de-doped by stirring in a solution of hydrazine hydrate (13 mL, 0.27 mol) and water (27 mL), washed thoroughly with methanol, and dried in vacuo to produce a yellow powder (0.42 g, 70%). Anal. Calcd for $(C_{11}H_{12}S)_n$: C, 75.00; H, 6.82; S, 18.20. Found: C, 74.16; H, 7.93; S, 17.72; Fe, 0.21; Cl, 0.75.

Poly[1,4-bis(3-octyl-2-thienyl)phenylene] (PBTBC$_8$). PBTBC$_8$ was synthesized in 82% yield in the same way as PBTBC$_4$ starting from BTBC$_8$. Anal. Calcd for $(C_{15}H_{20}S)_n$: C, 77.59; H, 8.17; S, 13.79. Found: C, 75.96; H, 8.87; S, 14.13; Fe, 0.19; Cl, 1.26.

Poly[1,4-bis(3-dodecyl-2-thienyl)phenylene] (PBTBC$_{12}$). PBTBC$_{12}$ was synthesized in 78% yield similar to PBTBC$_4$. Anal. Calcd for $(C_{19}H_{28}S)_n$: C, 79.17; H, 9.72; S, 11.11. Found: C, 77.96; H, 10.12; S, 11.36; Fe, 0.22; Cl, 2.82.

Poly(3-butyl-2,5-thienylene-*alt*-1,4-phenylene) (PBTC$_4$). BuLi (3.16 mL, 1.6 M in hexane, 5.06 mmol) and THF (0.5 mL) was added at −78 °C to an oven-dried 10 mL one-necked flask equipped with a magnetic stirrer and a condenser capped with a rubber septum. DBBTBC$_4$ (1.28 g, 2.50 mmol) dissolved in THF (4 mL) was then introduced into the flask, and the mixture was stirred at −78 °C for 15 min and then at −40 °C for another 15 min. The solution was then cooled to −60 °C, and magnesium bromide etherate (7 mmol) was added. The mixture was warmed gradually to −5 °C and stirred for 1 h, and then a mixture of 1,4-dibromobenzene (0.59 g, 2.5 mmol) and Ni(dppp)Cl_2 (0.013 g, 0.024 mmol) in THF (2 mL) was introduced. After being stirred at room temperature for 24 h under nitrogen, the reaction mixture was poured into a slightly acidified methanol solution and precipitated overnight. A brownish yellow solid polymer was collected and washed with methanol, water and methanol. The final product was purified by Soxhlet extraction with methanol for 24 h and then acetone for 4 h and dried in a high vacuum (0.43 g, 40% yield). Anal. Calcd for $(C_{14}H_{14}S)_n$: C, 76.91; H, 6.41; S, 14.65. Found: C, 71.84; H, 6.85; S, 15.20; Br, 3.30.

Poly(3-octyl-2,5-thienylene-*alt*-1,4-phenylene) (PBTC$_8$). PBTC$_8$ was produced in 61% yield in the same way as PBTC$_4$. Anal. Calcd for $(C_{18}H_{22}S)_n$: C, 80.00; H, 8.15; S, 11.85. Found: C, 74.88; H, 9.79; S, 12.02; Br, 2.67.

Table 4. Elemental Analysis Results

sample	expected composition	bulk composition from elemental analysis
PBTC$_4$	$C_{14}H_{14}S_1$	$C_{12.60}H_{14.42}S_{1.00}Br_{0.080}$ $C_{13.04}H_{13.80}S_{1.00}Fe_{0.33}Cl_{11.46}$[a]
PBTC$_8$	$C_{18}H_{22}S_1$	$C_{16.61}H_{26.00}S_{1.00}Br_{0.090}$ $C_{11.99}H_{20.43}S_{1.00}Fe_{0.33}Cl_{1.23}$[a]
PBTC$_{12}$	$C_{22}H_{30}S_1$	$C_{20.16}H_{37.10}S_{1.00}Br_{0.10}$ $C_{17.34}H_{35.10}S_{1.00}Fe_{0.45}Cl_{1.92}$[a]
PBTBC$_4$	$C_{22}H_{24}S_2$	$C_{23.41}H_{25.02}S_{2.00}Cl_{0.076}$ $C_{21.36}H_{27.72}S_{2.00}Fe_{0.56}Cl_{2.30}$[a]
PBTBC$_8$	$C_{30}H_{40}S_2$	$C_{28.70}H_{40.24}S_{2.00}Cl_{0.080}$ $C_{27.82}H_{45.10}S_{2.00}Fe_{0.66}Cl_{2.24}$[a]
PBTBC$_{12}$	$C_{38}H_{56}S_2$	$C_{36.62}H_{57.12}S_{2.00}Cl_{0.22}$ $C_{36.68}H_{55.50}S_{2.00}Fe_{0.68}Cl_{2.56}$[a]

[a] Powder sample chemically doped by $FeCl_3$.

Poly(3-dodecyl-2,5-thienylene-*alt*-1,4-phenylene)(PBTC$_{12}$). PBTC$_{12}$ was synthesized and purified similarly as PBTC$_4$ and obtained as a yellow solid in 50% yield. Anal. Calcd for $(C_{22}H_{30}S)_n$: C, 80.98; H, 9.20; S, 9.82. Found: C, 74.96; H, 9.96; S, 8.59; Br, 2.55.

Electrochemical Polymerization of PBTBC$_n$ Polymers. PBTBC$_n$ polymer films were electrochemically generated on an ITO glass electrode (resistance ca. 240 Ω) by either the cyclic voltammetric (CV) or galvanostatic method under an argon atmosphere. All experimental values were corrected to SCE. Thin polymer films were preferably grown galvanostatically from monomer solutions (0.02−0.05 M) in 0.1 M supporting electrolyte (Bu_4NBF_4) in acetonitrile at a current density of 0.5 mA cm^{-2}.

Polymer Doping. Polymers were doped by placing polymer pallets (ca. 0.1 g) in a vessel containing ground iodine crystals in the dark, or by stirring the polymer powder (ca. 0.1 g) in a large volume (ca. 100 mL) of 0.1 M $FeCl_3$ in dry nitromethane for 40 min.

Results and Discussion

Physical Properties. PBTC$_8$ and PBTC$_{12}$ are yellow powders, similar to PBTC$_4$ reported previously.[9] PBTC$_n$ are more soluble in common organic solvents than their PBTBC$_n$ analogues. The number-averaged molecular weights (M_n)/polydispersity indexes (PDI) for PBTC$_8$ and PBTC$_{12}$ are 5400/1.6 and 4300/1.3 respectively, relative to polystyrene. This suggests that Grignard coupling produces lower molecular weight PBTC$_n$ with a narrower molecular weight distribution than the $FeCl_3$ route to PBTBC$_n$ reported previously.[13]

While PBTBC$_n$ are all conductive when doped by I_2, it is quite difficult to measure the corresponding conductivity for PBTC$_8$ or PBTC$_{12}$ because of difficulty in pressing a pellet from either of them as they stick to the surface of the circular metal die. The only measurable conductivity is 2.4 $\times 10^{-4}$ S cm^{-1} for PBTC$_4$.[9]

The bulk composition figures of neutral polymers as determined by microanalysis are in reasonable agreement with the theoretical values. For $FeCl_3$-doped PBTBC$_n$, the results in Table 4 suggest that every repeating unit is associated with approximately 0.56−0.68 $FeCl_4^-$ dopant. The ring-to-anion ratio in electrochemically or chemically synthesized polypyrrole, polymethylthiophene, and polythiophene[15−17] was around 0.3.

Neutral PBTC$_n$ polymers form good films when cast from high boiling point solvents, such as xylene, and have smooth surfaces similar to that reported for $FeCl_3$-synthesized poly(dodecylthiophenes) (PDDT) or totally regioregular poly(hexylthiophenes) (PHT).[18] When the polymers are doped, the morphology of all the samples becomes more granular, as commonly observed.[19,20]

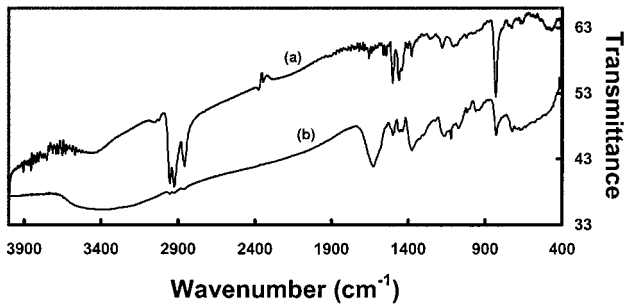

Figure 1. FTIR spectra of (a) neutral $PBTBC_4$ and (b) $FeCl_3$-doped $PBTBC_4$.

Structure Characterization. The polymer structures are verified by NMR and FTIR spectra (the peaks are listed in Tables 1−3). $PBTBC_n$ exhibit almost identical ^1H NMR chemical shifts as their $PBTC_n$ analogues in both the aromatic and aliphatic resonance regions, except the lack of a multiplet at about δ 7.64 ppm, ascribed to the terminal 4-bromo-1-phenylene units in $PBTC_n$ polymers. The relative intensity of the C_β−H resonance on the internal thiophene ring at δ 7.10 ppm is also increased in the ^1H NMR spectra for $PBTBC_n$. All these results indicate that the $PBTC_n$ and $PBTBC_n$ polymers have the expected 2,3,5-trisubstituted thiophene units and 1,4-disubstituted benzene rings in their polymer backbones.

The FTIR spectra for neutral and doped $PBTBC_4$ are shown in Figure 1, parts a and b, respectively. The stretching vibrations at 1440−1500 and 1605, 1543 cm^{-1} are consistent with the presence of thienylene and phenylene moieties. The vibration bands at around 830 cm^{-1} for C_β−H out of plane bending and at 3054 cm^{-1} for C_β−H stretching are indicative of a 2,3,5-trisubstituted thiophene, in agreement with the results from NMR studies. The stretching at about 873 cm^{-1} manifests the *para*-substitution pattern of the benzene ring. The CH_3− and −CH_2− stretching at 2953 and 2922 cm^{-1} indicate the existence of alkyl chains. When the polymer is doped, e.g., by $FeCl_4^-$, the stretching vibrations in the region 800−1700 cm^{-1} become broad (see Figure 1b) due to the positively charged state of the polymer backbone. The relative intensities of stretches at 835, 2922, and 2955 cm^{-1} are all greatly reduced because of "the rise of baseline", a result of the enhanced absorption in the IR region due to the formation of polaron and bipolaron.

Optical Properties. Table 5 summarizes the UV−vis absorption maxima and fluorescence maxima for the $PBTC_n$ series. The data for the $PBTBC_n$ series are also included for comparison, although they have been reported previously.[9,13] Both $PBTC_8$ and $PBTC_{12}$ have a maximum absorption (λ_{max}) at 386 nm in $CHCl_3$, which is blue shifted in comparison to that of analogues $PBTBC_8$ and $PBTBC_{12}$. This suggests that the backbone of $PBTC_n$ is more twisted in solution. The difference in λ_{max} is very small between the $PBTC_n$ film sample and in $CHCl_3$. The absorption maximum is at around 388 nm for both $PBTC_8$ and $PBTC_{12}$ films and $CHCl_3$ solution, which suggests that the $PBTC_n$ series has a greater torsional angle or shorter mean conjugation length.[21]

For $PBTC_n$ polymers, the emission peak positions (λ_{em}) in the film samples red-shift going from $PBTC_4$ to $PBTC_8$. The $PBTC_n$ film samples also are generally red shifted in λ_{em} relative to their solution samples. This is due to a very slight increase in the coplanarity in the film samples, especially those with longer chains, compared to the more random conformation in solution. The modification of the polymer backbone, and hence the decrease in coplanarity in $PBTC_n$, also increases both the quantum yield and optical band gap compared to $PBTBC_n$.

Table 5. Summary of UV−vis and Luminescence Results

sample		λ_{max} (nm) UV−vis	λ_{max} (nm) emission	quantum yield[a] (%)	optical band gap (eV)
solution	$PBTC_4$	388	488	48	
	$PBTC_8$	386	488	66	
	$PBTC_{12}$	386	488	69	
	$PBTBC_4$	398	492	26	
	$PBTBC_8$	398	494	23	
	$PBTBC_{12}$	398	494	19	
film	$PBTC_4$	395	504	17	2.57
	$PBTC_8$	388	512		2.64
	$PBTC_{12}$	388	512		2.68
	$PBTBC_4$	420	512		2.58
	$PBTBC_8$	420	521		2.58
	$PBTBC_{12}$	422	529		2.58

[a] Solution values in $CHCl_3$ with quinine sulfate in 0.1 M H_2SO_4 as reference.

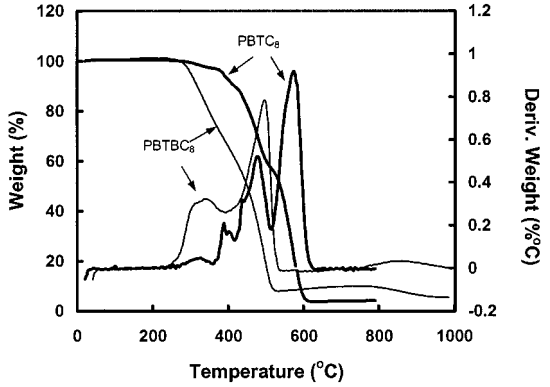

Figure 2. TG and DTG plots of $PBTC_8$ and $PBTBC_8$ in air.

Thermal Stability. Kinetic studies of the thermal decomposition of the $PBTBC_n$ polymers showed that they are more thermally stable, particularly in the doped state, than polyalkylthiophenes.[22] The TG thermocurves of $PBTC_n$ in N_2 show a degradation pattern very similar to those of their $PBTBC_n$ analogues. This is expected due to the similarity between the two polymer structures.

A typical comparison of thermocurves of $PBTC_8$ and $PBTBC_8$ in air and their corresponding DTG curves is shown in Figure 2. $PBTC_8$ and $PBTBC_8$ decompose in two major steps by degradation of the side chains, and second by decomposition of polymer backbone. From the DTG curves, a multiple-step scission profile observable in the first main step of decomposition of the polymers, especially of $PBTC_8$, suggests that the degradation of side chains is stepwise and starts with small fragments, such as CH_3− or C_2H_5−. However, the gradual loss of side chains is much slower in $PBTC_8$ than in $PBTBC_8$, although the onset is about the same. This enhances the thermal stability of $PBTC_8$, in comparison with $PBTBC_8$. $PBTC_4$ and $PBTC_{12}$ are also more thermally stable than their analogues.

The reason for the enhancement of thermal oxidative stability of $PBTC_n$ over $PBTBC_n$ may be the higher purity of $PBTC_n$ than $PBTBC_n$. Elemental analysis of $PBTBC_n$ shows that this series of polymers all contain residue iron from the polymerization step. Although the

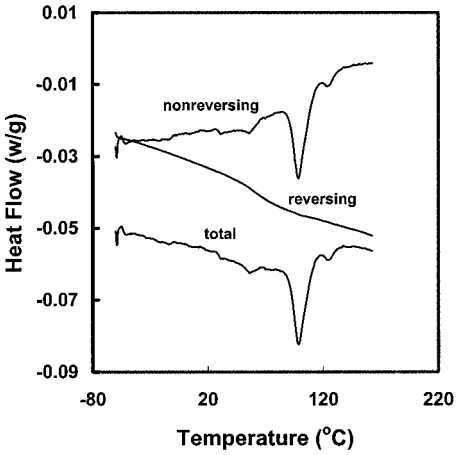

Figure 3. Deconvoluted MDSC curves of $PBTC_4$.

Table 6. MDSC Data for Neutral $PBTC_n$ and $PBTBC_n$ Polymers

polymer	T_g (°C)	$T_{m,1}$ (°C)	$T_{m,2}$ (°C)	T_c (°C)
$PBTC_4$	58.3	54.6	99.9	124.3
$PBTC_8$	−4.0	42.6	60.5	78.7
$PBTC_{12}$	−19.2	50.2	67.4	85.7
$PBTBC_4$	122.3			
$PBTBC_8$	50.4			
$PBTBC_{12}$	59.6			

content of iron is not high (0.2 w/w), it may serve as an initiator[23] and/or a catalyst[24] for the thermal oxidative decomposition.

Liquid Crystalline Property and Glass Transition. All of the polymers studied here were first examined by normal DSC, but accurate, reliable, and reproducible results are sometimes difficult to obtain due to the very small heat of reaction and overlapping of the thermal transitions. A new dynamic technique, modulated differential scanning calorimetry (MDSC),[25,26] was employed in this study. The raw data in MDSC can be deconvoluted using discrete Fourier transformation software to obtain a conventional DSC curve (total) and/or both its reversing and nonreversing components.

Figure 3 shows the deconvoluted MDSC curves for polymer $PBTC_4$. No resolvable glass transition is observed from the total curve, which is the same as normal DSC. However, a distinct glass transition at 58 °C (T_g) is observed from the reversing component. The nonreversing curve shows three endothermic events at 54.6, 99.9, and 124.3 °C, respectively. Since paraffin side chains melt typically around 40−50 °C,[27] the first transition is assigned to the melting of side chains ($T_{m,1}$) although the substituent chain is quite short. Similar thermal behavior was observed in poly(3-decyllthiophenes)[28] and polymers with similar structure but substituted by C_5H_{11} groups.[2] The second endothermic transition is very strong and is ascribed to the melting of polymer backbone ($T_{m,2}$), as suggested by other reports.[29−31] The third endothermic event following the two melting transitions is assigned to the transition from a metastable liquid crystalline phase to an isotropic phase (T_c). The liquid crystalline feature had been reported for other comblike polymers which consist of rigid backbone and flexible side chain,[1,2,11,29−31] similar to the present series of polymers.

Table 6 summarizes the thermal events evaluated by MDSC curves for all the polymers studied in this work. $PBTC_8$ and $PBTC_{12}$ show three endothermic events but the glass transition temperatures decrease with an increase in alkyl side chain length. For the $PBTBC_n$ series, melting transitions can sometimes be observed in MDSC but are quite weak and not exactly reproducible due to the low degree of crystallinity in the polymer. However, the reversing curve for $PBTBC_4$ shows a very sharp glass transition at 122 °C while those for $PBTBC_8$ and $PBTBC_{12}$ are much lower at 50.4 and 59.6 °C, respectively. The T_g for $PBTBC_{12}$ is slightly higher than that of $PBTBC_8$, a possible result of the stronger interaction (overlapping and locking) of the longer alkyl side chains. However, the T_gs for $PBTBC_n$ are all higher than their $PBTC_n$ counterparts. The reason may be that the greater degree of interaction of the alkyl side chains in $PBTBC_n$ due to their closer proximity, making it more difficult for the C−C bonds in the $PBTBC_n$ backbone to rotate.

The liquid crystalline properties for $PBTC_n$ polymers are confirmed by polarized optical microscopy study. An anisotropic orientation is observed when the samples are heated to melt ($T_{m,2}$), as shown in Figure 4. An isotropic phase emerges when the temperature is higher than T_c but the transition is reversible as liquid crystalline phase comes back when the temperature is lowered than T_c.

XRD measurements verified the semicrystalline nature of $PBTC_n$ polymers. Figure 5 shows the powder XRD pattern for $PBTC_{12}$ as an example. All the polymers are partially crystalline as suggested by the XRD pattern. Polymers substituted by longer chains exhibited more and sharper reflection peaks, just like the polyalkylthiophene systems.[32,33] The strong reflections at low angles together with their higher orders indicate a layered structure with large length scale periodicity. The XRD diffraction peak angles and their corresponding spacings are listed in Table 7.

The distinct diffraction peaks at lower angles are due to interlayer spacing of 8.81, 13.20, and 16.66 Å for $PBTC_4$, $PBTC_8$, and $PBTC_{12}$, respectively. In polyalkylthiophene systems, especially in the model developed by Winokur et al.,[34] the reflections at low angles are usually assigned to the reflections of interchain spacing. If the model is applicable to the present polymer structure, the spacing values between polymer chains are 8.81, 13.20, and 16.66 Å for $PBTC_4$, $PBTC_8$, and $PBTC_{12}$, respectively. However, the interchain spacing is lower than that of the corresponding polyalkylthiophenes, whose values are 13.18, 20.53, and 26.43 Å for butyl-, octyl-, and dodecyl-substituted polythiophenes, respectively.[32] This is because the phenylene rings incorporated in the present polymers are unsubstituted, providing more space to facilitate the side chain interdigitation and overlapping.

$PBTBC_n$ polymers exhibit broad amorphous scattering with only one ill-defined peak at low angles discernible for $PBTBC_8$ and $PBTBC_{12}$. This is consistent with the results from MDSC: $PBTBC_n$ polymers have no melting transition. The amorphous behavior of $PBTBC_n$ series parallels the amorphous nature of regioregular HH−TT poly(3-alkylthiophenes) vs HT poly(3-alkylthiophenes).[36]

XPS. The electronic environments of the neutral and doped polymers were studied by XPS similar to earlier reports.[37−38] The S(2p) and Cl(2p) core level spectra of both the neutral and $FeCl_3$-doped $PBTC_4$ are shown in Figure 6. The S(2p) spectra of neutral polymers are also included for comparison.

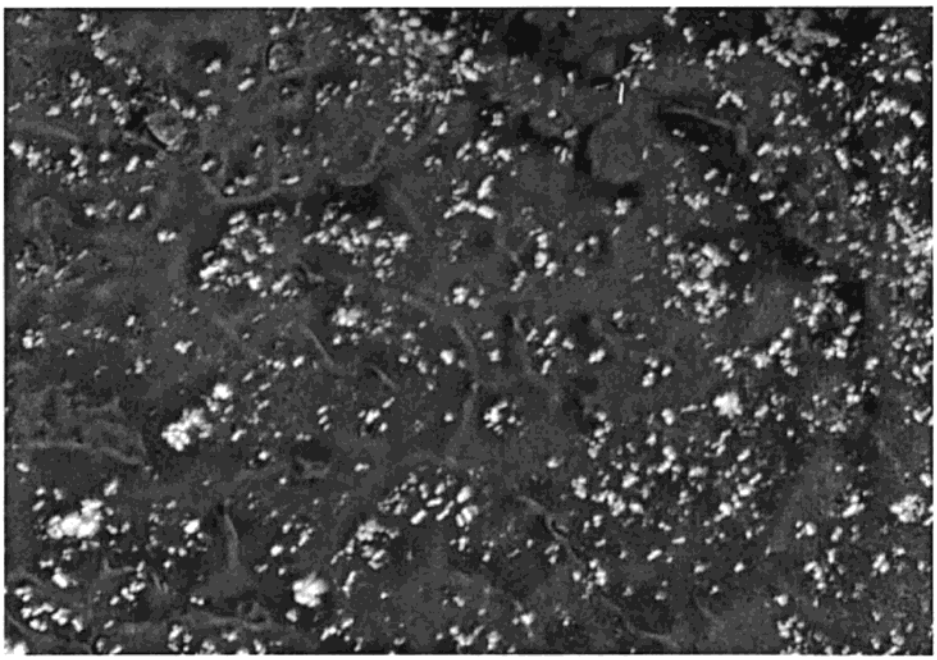

Figure 4. Optical polarized photography of $PBTC_4$ at 97 °C.

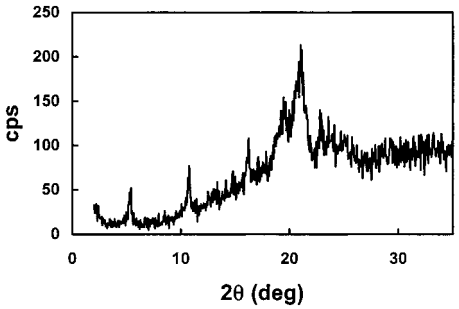

Figure 5. XRD diffraction pattern of $PBTC_{12}$.

Table 7. XRD Diffraction Angle (2θ) and Spacing (d) for $PBTC_n$ Polymers

polymer	2θ (deg)	d (Å)
$PBTC_4$	10.02	8.81
	20.45	4.34
	21.27	4.17
	22.30	3.98
$PBTC_8$	6.73	13.10
	13.31	6.64
	20.34	4.36
	21.41	4.14
	22.50	3.94
$PBTC_{12}$	5.30	16.66
	10.70	8.25
	16.12	5.49
	20.95	4.23
	21.32	4.15
	22.80	3.90

The S(2p) component deconvolutions for neutral polymers (Figure 6a) reveal only one spin−orbit splitting doublet [$S(2p_{3/2})$ and $S(2p_{1/2})$], the binding energy between them, ΔE, is about 1.2 eV with the $S(2p_{3/2})$ peak BE at about 163.8 eV and an intensity ratio of 2:1, which is due to the sulfur species in the thiophene ring. However, two doublets are deconvoluted from the S(2p) spectra for the $FeCl_3$-doped samples (Figure 6b) with the BE of $S(2p_{3/2})$ located at 163.8 and 164.8 eV, respectively. While the former electronic environment originates similarly as in the neutral polymer, the latter suggests that some of the sulfur atoms are positively polarized or partially charged, a result of the oxidation of the polymer chain by dopants.[17] The ratios of the polarized sulfur to total sulfur are shown in Table 8.

In the $FeCl_3$-doped sample, the Cl(2p) envelope can be fitted into three spin−orbit splitting doublet [$Cl(2p_{3/2})$ and $Cl(2p_{1/2})$, $\Delta E = 1.6$ eV] (Figure 6c) with the expected intensity ratio of 2:1 and BEs for $Cl(2p_{3/2})$ at 198.4, 200.0, and 201.0 eV, respectively. The main peak component with a $Cl(2p_{3/2})$ BE at 198.4 eV is attributable to the formation of $FeCl_4^-$ species.[39] This is consistent with the presence of an $Fe(2p_{3/2})$ component with a BE in the 711.0 eV region (not shown), characteristic of the metal halide species.[40] The component with a $Cl(2p_{3/2})$ BE at 200.0 eV, accounting for 18−35% of the total chlorine species, is probably associated with the C−Cl species,[41] which is due to the chlorination of the polymer backbone during doping. The exact identity of the weak $Cl(2p_{3/2})$ peak component at about 201.0 eV is unknown. It may be ascribed to $FeCl_4^-$ anions physically close to a positively charged sulfur atom.

Table 8 gives the % of charged sulfur determined by XPS for the various polymers. The ratios of $[S^+]/[S]$ agree fairly well with the doping levels determined by elemental analyses (see Table 4). The conductivity of the I_2-doped polymers increases with an increase in the doping level.

Electrochemistry. Electrochemical Polymerization. $BTBC_n$ can also be anodically electropolymerized (denoted as $ePBTBC_n$) using galvanostatic and cyclic voltammetric methods, but $ePBTBC_n$ films for CV studies were preferably polymerized in the galvanostatic mode as this method was more efficient. The three polymers have been prepared as thin films on ITO glass using a constant deposition charge of 15 mC cm^{-2} and a constant current density of 0.5 mA cm^{-2} at a monomer concentration of 0.01 M. Working potentials for the three polymerizations are in the range +1.3 to +1.4 V. UV−vis absorbance at peak positions are 0.093, 0.24, and 0.46 for $ePBTBC_4$, $ePBTBC_8$, and $ePBTBC_{12}$ respectively, indicating a higher polymerization yield for $ePBTBC_{12}$. This is consistent with the observations

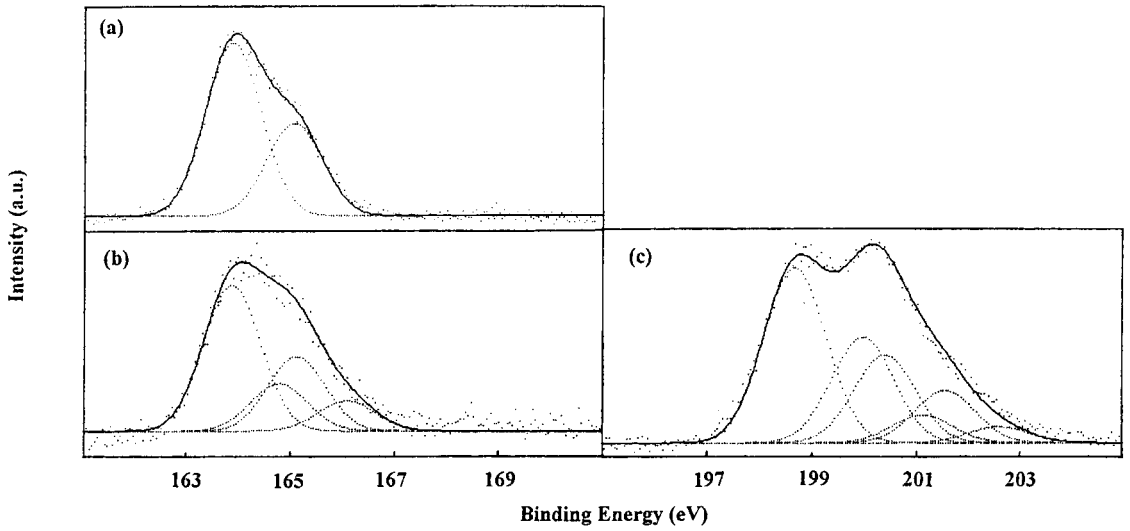

Figure 6. XPS spectra of $PBTC_4$: (a) S(2p) spectrum of neutral polymer; (b) S(2p) spectrum of $FeCl_3$-doped polymer; (c) Cl(2p) spectrum of $FeCl_3$-doped polymer.

Table 8. Doping Level and Conductivity (σ) of Polymers

		σ (S cm^{-1})	
sample	$[S_r+]/[S]$ (%)	$FeCl_3$-doped	I_2-doped
$PBTBC_4$	33	1.1×10^{-3}	2×10^{-1}
$PBTBC_8$	32	*a*	7×10^{-2}
$PBTBC_{12}$	31	*a*	1.5×10^{-2}
$PBTC_4$	25	1.0×10^{-3}	7.4×10^{-4}
$PBTC_8$	25	2.0×10^{-3}	*b*
$PBTC_{12}$	22	3.8×10^{-3}	*b*

[a] The $FeCl_3$-doped polymers are too brittle for the conductivities to be measured. [b] The pellets of the polymers are difficult to compress as the T_gs are lower than room temperature.

obtained in cyclic voltammetric polymerization (not shown) and reported by other workers.[42]

Cyclic Voltammetry of the Polymer. The discovery that polyheterocycles can be switched between an oxidized, anodically conducting (p-doped) form and a neutral, insulating form has opened a new field of study in material science and electrochemistry.[43] Much effort is stimulated by the recognition that these conducting polymers could find eventual applications in battery[44] and molecular electronic devices.[45] However, n-type doping of conjugated polymers is not as well documented as p-type due to the instability of polymers at high negative potentials. It has attracted greater attention in recent years because of its potential application in microelectronics[46,47] and electrochemical capacitors.[48] Polymers exhibiting concurrent p- and n-dopability can be used in high-density capacitors[48] and electrochromic devices.[49]

Figure 7 shows the CV plots for $ePBTBC_8$, $ePBTBC_4$, and $PBTC_4$ as representatives, which manifest both p- and n-dopability in 1 M Bu_4NBF_4 in acetonitrile.[50] The cyclic voltammogram of $ePBTBC_8$ (Figure 7a) shows two oxidation processes accompanied by a color change from yellow → dark blue → purple. Upon reverse scanning, only one dedoping peak is resolved with color recovering from purple to yellow. The line shape of $ePBTBC_8$ is between those of $ePBTBC_4$ (Figure 7b) and $ePBTBC_{12}$ (not shown). We attribute these two oxidation processes to the separation of neutral-to-polaron and polaron-to-bipolaron charge carrier formation events but the formation of bipolaron in $ePBTBC_4$ is accompanied by a serious overoxidation of the polymer film as indicated by the lack of reduction peak upon back sweeping when

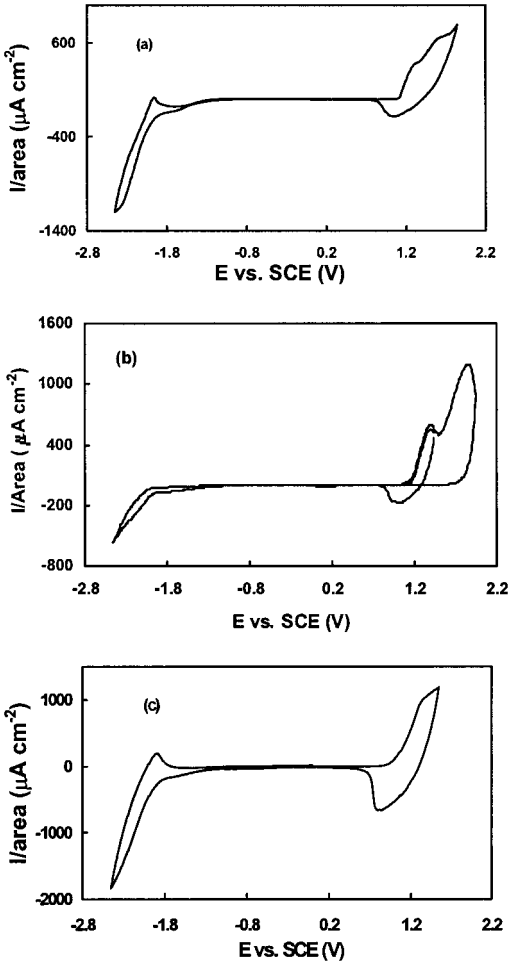

Figure 7. Cycilc voltammetry of (a) $ePBTBC_8$, (b) $ePBTBC_4$, and (c) $PBTC_4$.

switched at +1.95 V. When the potential is scanned anodically to +1.4 V for $ePBTBC_4$, a narrow oxidation peak with the maximum at +1.25 V is obtained accompanied by a color change from yellow to dark blue. The sharp peak shape is very similar to that of poly(dibutylbithiophene),[51] manifesting a regular structure of the polymer.

Figure 7c shows the CV curves of $PBTC_4$ with a well-resolved one-electron process. In comparison, $PBTC_8$

Table 9. Summary of Onset Potential, Peak Potential, and Band Gap

	p-doping			n-doping			band gap	
polymer	E_{on} (V)	E_{pa} (V)	E_{pc} (V)	E_{on} (V)	E_{pc} (V)	E_{pa} (V)	$E_g{}^a$ (eV)	$E_g{}^b$ (eV)
$PBTC_4$	1.05	1.33	0.60	−1.87	−2.14	−1.88	2.92	2.57
$PBTC_8$	1.14	1.48	0.88	−1.88	−2.21	−1.86	3.02	2.64
$PBTC_{12}$	1.20	1.88	1.07, 1.61	−1.89	−2.32	−1.98	3.09	2.68
$ePBTBC_4$	1.02	1.25	1.02	−1.89	*c*	*c*	2.91	2.60
$ePBTBC_8$	1.11	1.31, 1.61	1.04	−1.81	−2.39	−1.96	2.92	2.59
$ePBTBC_{12}$	1.24	1.63	0.96	−1.75	−2.14	−1.94	2.91	2.58
$PBTBC_8$	1.11	1.48	0.70	−1.80	−2.14	−1.94	2.91	2.58

[a] Electrochemical band gap. [b] Optical band gap. [c] Unresolved.

displays a similar CV profile while $PBTC_{12}$ exhibits two ill-resolved one-electron processes in p-dedoping sweeping. Similar observations were reported by other researchers[42,52] and the reason is attributed to the difference in film thickness and morphology and hence the ease of diffusion of counterions through the polymer matrix. SEM studies show that $PBTC_4$, $PBTC_8$, and $PBTC_{12}$ have very compact and homogeneous surfaces but the film thickness of $PBTC_{12}$ is smaller due to its lower solubility as indicated by UV absorbance. The morphology of $ePBTBC_n$ films changes from granular to compact gradually on going from $ePBTBC_4$ to $ePBTBC_{12}$, as the thickness of the film increases with the decrease of polymer solubility in the electrolyte solution. Compact morphology also contributes to the "break-in" phenomenon[12,50] in n-doping process, which is more serious in $PBTC_n$ than in $ePBTBC_n$ polymers.

Table 9 summarizes the onset potentials and doping and dedoping peak potentials for both p- and n-doping processes. Also listed are the band gaps obtained both optically and electrochemically. It can be seen that both the onset and peak potentials of p-doping increase slightly with the increase of alkyl chain length for the two series of polymers, $ePBTBC_n$ and $PBTC_n$, similar to the report from other workers.[42] The influence of substituent chain length on the n-doping process is similar, i.e., to make the E_{on} shift anodically for the $ePBTBC_n$ polymer, but it is very weak for $PBTC_n$. The overall effect of alkyl chain length on the difference between p- and n-doping onset (E_g) is thus to make it slightly larger with the increase of alkyl chain size for the $PBTC_n$ series, but keeping it almost constant for $ePBTBC_n$. The optical E_gs show the same trend with the change of substituent length but are 0.3−0.4 eV lower than the electrochemical ones. One reason for the difference is that a high (1 M) electrolyte concentration was employed in this work. It is reported that high electrolyte concentration shifts the voltammetric wave anodically, and a difference about 0.05 V can be induced by a change of electrolyte concentration from 0.1 to 1 M.[53]

Electrochromism. Optoelectrochemistry, in which UV−vis−NIR spectra were obtained as a function of applied potential, provides a more probing and convincing measurement of the in situ electronic band structure during electrochemical oxidation or reduction. All the polymers electrochemically studied previously exhibit electrochromism with a color change from near transparent yellow for neutral polymers to opaque black for p-doped polymers. A dramatic change in absorption spectra was observed during doping process and an example is given for $PBTC_8$ as shown in Figure 8. Two additional potential-dependent absorption peaks are observed at 600 nm (2.06 eV) and a wavelength longer than 1400 nm (<1.1 eV) with the increase of potential.

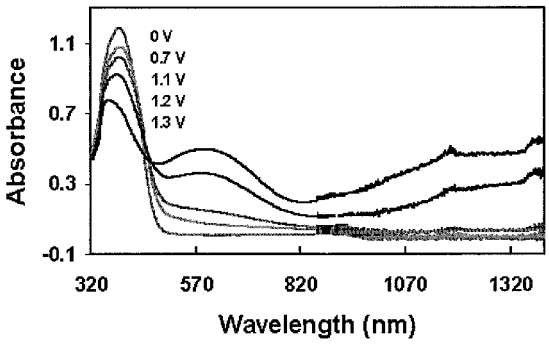

Figure 8. In situ potential dependent UV−vis−NIR spectra of $PBTC_8$ during p-doping process.

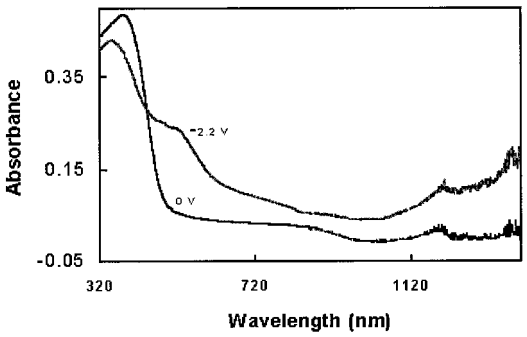

Figure 9. In situ potential dependent UV−vis−NIR spectra of $ePBTBC_8$ during n-doping process.

The emergence of the two midgap absorption peaks is consistent with the formation of bipolaronic charge carriers and is accompanied by a lowering of the absorbance and a blue shift of $\pi-\pi^*$ transition as the formation of intragap sates is accompanied by a change of band structure.[52,54,55] Structurally similar polymers were reported by Reynolds et al.[10] to show very similar band gaps and intragaps.

The electrochromic phenomenon of n-doping has also been examined for $ePBTBC_8$, as shown in Figure 9. Two new transitions at about 515 and >1400 nm are observed together with a decrease in intensity and a blue shift of the $\pi-\pi^*$ transition. The intragap states are thus slightly farther from the band edges in the n-doped polymer than in the p-doped one. This result is the same as that reported by Reynolds et al.,[54] for which a larger degree of distortion in n-doping than in p-doping is assumed to be responsible.

Conclusions

Two series of regioregular polymers consisting of phenylene and substituted thienylene ($PBTC_n$) or bithienylene ($PBTBC_n$) repeating units have been chemically or electrochemically synthesized and characterized. The length of substituent exerts similar effects on both series

of polymers but $PBTC_n$ polymers have better solubility in organic solvents and show a better film forming ability than the corresponding chemically produced $PBTBC_n$. A blue shift in their absorption and fluorescence maximum, a higher fluorescence quantum yield and a lower conductivity with reference to $PBTBC_n$ have been observed, attributable to the decrease of ratio of thiophene to benzene rings in the polymer backbone and hence an increase of twisting of neighboring aromatic units. The $PBTC_n$ polymers are partially crystalline and show liquid crystalline properties as indicated by MDSC and XRD results. Their glass transition temperatures are lower than those of the $PBTBC_n$ analogues, and their thermal stabilities in air are improved in comparison with $PBTBC_n$. FTIR and XPS investigations show that doping induced the formation of positively charged sulfur species in both series of polymers. Polarons and bipolarons are shown to be the main charge carriers by UV−vis absorption spectral data and CV in both the p- and n-doping processes.

Acknowledgment. Financial support from the National University of Singapore (NUS) under Research Grant RP960613 is gratefully acknowledged. J.M.X. is grateful to the NUS for the award of a research scholarship.

References and Notes

(1) Bao, Z.; Chan, W. K.; Yu, L. *J. Am. Chem. Soc.* **1995**, *117*, 12426.
(2) Saadeh, H.; Goodson III, T.; Yu, L. *Macromolecules* **1997**, *30*, 4608.
(3) Tanigaki, N.; Masuda, H.; Kaeriyama, K. *Polymer* **1997**, *38*, 1221.
(4) Fahlman, M.; Birgersson, J.; Kaeriyama, K.; Salaneck, W. R. *Synth. Met.* **1995**, *75*, 223.
(5) Pelter, A.; Rowlands, M.; Jenkins, I. H. *Tetrahedron Lett.* **1987**, *43*, 5213.
(6) Pelter, A.; Maud, J. M.; Jenkins, I. H.; Sadeka, C.; Coles, G. *Tetrahedron Lett.* **1989**, *30*, 3461.
(7) Yamamoto, T.; Morita, A.; Miyazaki, Y.; Maruyama, T.; Wakayama, H.; Zhou, Z.; Nakamura, Y.; Kanbara, T.; Sasaki, S.; Kubota, K. *Macromolecules* **1992**, *25*, 1214.
(8) Yamamoto, T.; Zhou, Z.; Kanbara, T.; Shimura, M.; Kizu, K.; Maruyama, T.; Nakamura, Y.; Fukuda, T.; Lee, B.; Ooba, N.; Tomaru, S.; Kurihara, T.; Kaino, T.; Kuboto, K.; Sasaki, S. *J. Am. Chem. Soc.* **1996**, *118*, 10389.
(9) Ng, S. C.; Xu, J. M.; Chan, H. S. O. *J. Mater. Chem.* **1999**, *9*, 381.
(10) Reynolds, J. R.; Ruiz, J. P.; Child, A D.; Nayak, K.; Marynick, D. S. *Macromolecules* **1991**, *24*, 678.
(11) Ruiz, J. P.; Dharia, J. R.; Reynolds, J. R.; Buckley, L. J. *Macromolecules* **1992**, *25*, 849.
(12) Jenkins, I. H.; Salzner, U.; Pickup, P. G. *Chem. Mater.* **1996**, *8*, 2445.
(13) Ng, S. C.; Xu, J. M.; Chan, H. S. O. *Synth. Met.* **1998**, *92*, 33.
(14) McCullough, R. D.; Lowe, R. D.; Jayaraman, M.; Anderson, D. L. *J. Org. Chem.* **1993**, *58*, 904.
(15) Bach, M. G. C.; Reynolds, J. R. *J. Phys. Chem.* **1994**, *98*, 13636.
(16) Pfluger, P.; Street, G. B. *J. Chem. Phys.* **1984**, *80*, 544.
(17) Kang, E. T.; Neoh, K. G.; Tan, K. L. *Phys. Rev. B* **1991**, *44*, 10461.
(18) McCullough, R.D.; Ewbank, P. C. In *Handbook of Conducting Polymers*; Skotheim, T., Eelsenbaumer, R. L., Reynolds, J. R., Eds.; Marcel Dekker: New York, Basel, Switzerland, and Hong Kong, 1998; pp 242 and 245.
(19) Hagiwara, T.; Yamaura, T.; Sato, K.; Hirasaka, M.; Itawa, K. *Synth. Met.* **1989**, *32*, 367.
(20) Nicolau, Y. F.; Moser, P. *J. Polym. Sci., Part B: Polym. Phys.* **1993**, *31*, 1529.
(21) Souto Maior, R. M.; Hinkelmann, K.; Eckert, H.; Wudl, F. *Macromolecules* **1990**, *23*, 1268.
(22) Ng, S. C.; Xu, J. M.; Chan, H. S. O. *Synth. Met.* **2000**, *110*, 31.
(23) MacCallum, J. R. In *Comprehensive Polymer Science*, 1st ed.; Allen, S. G., Bevington, J. C., Eds.; Pergamon Press: Oxford, England, New York, Beijing, Frankfurt, Germany, Sao Paulo, Brazil, Sydney, Australia, Tokyo, and Toronto, Canada, 1989; Vol. 6, Chapter 18, p 536.
(24) Hawkins, W. Lincoln *Polymer Degradation and Stabilisation*; Springer-Verlag: Berlin and New York, 1984; Chapter D, p 52.
(25) Reading, M.; Elliott, D.; Hill, V. L. *J. Therm. Anal.* **1993**, *40*, 949.
(26) Reading, M.; Luget, A.; Wilson, R. *Thermochim. Acta* **1994**, *238*, 295.
(27) Plate, N. A.; Shibaev, V. P. *Comb-shaped polymers and liquid crystals*; Plenum Press: New York and London, 1987; Chapter 6, p 2120.
(28) Meille, S. V.; Romita, V.; Caronna, T.; Lovinger, A. J.; Catellani, M.; Belobrzeckaja, L. *Macromolecules* **1997**, *30*, 7898.
(29) Yu, L.; Bao, Z. *Adv. Mater.* **1994**, *6*, 156.
(30) Bao, Z.; Chen, Y.; Cai, R.; Yu, L. *Macromolecules* **1993**, *26*, 5281.
(31) Yu, L.; Bao, Z.; Cai, R. *Angew. Chem., Int. Ed. Engl.* **1993**, *32*, 1345.
(32) Kawai, T.; Nakazono, M.; Yoshino, K. *Technol. Rep. Osaka Univ.* **1992**, *42*, 297.
(33) Chen, T.; Wu, X.; Rieke, R. D. *J. Am. Chem. Soc.* **1995**, *117*, 233.
(34) Winokur, M. J.; Mamsley, P.; Moulton, J.; Smith, P.; Heeger, A. J. *Macromolecules* **1991**, *24*, 3812. (b) Winokur, M. J.; Spiegel, D.; Kim, Y.; Hotta, S.; Heeger, A. J. *Synth. Met.* **1989**, *28*, C419.
(35) Gustafsson, G.; Inganas, O.; Osterholm, H.; Laakso, H. *Polymer* **1991**, *32*, 1574.
(36) Mao, H.; Xu, B.; Holdcroft, S *Macromolecules* **1993**, *26*, 1163.
(37) Chan, H. S. O.; Ng, S. C.; Sim, W. S.; Seow, S. H.; Tan, K. L.; Tan, B. T. G. *Macromolecules* **1993**, *26*, 144.
(38) Ng, S. C.; Chan, H. S. O.; Miao, P.; Tan, K. L. *Synth. Met.* **1997**, *90*, 25.
(39) Furlani, A.; Russo, M. V.; Polzonetti, G.; Martin, K.; Wang, H. H.; Ferraro, J. R. *Appl. Spectrosc.* **1990**, *44*, 331.
(40) Moulder, J. F.; Stickle, W. F.; Sobol, P. E.; Bomben, K. D. *Handbook of X-ray Photoelectron Spectroscopy*; Perkin-Elmer: Eden Prairie, MN, 1992; p 60.
(41) Clark, D. T.; Kilcast, D.; Admas, D. B.; Musgrave, W. K. R. *J. Electron. Spectrosc.* **1975**, *6*, 117.
(42) Roncali, J.; Garreau, R.; Yassar, A.; Marque, P.; Garnier, F.; Lemaire, M. *J. Phys. Chem.* **1987**, *91*, 6706.
(43) Margolis, J. M. *Conducting Polymers*; Chapman and Hall: New York, 1989; p 1.
(44) Scrosati, B. *Proc. Solid State Chem.* **1988**, *18*, 1.
(45) Guay, J.; Diaz, A.; Wu, R.; Tour, J. M. *J. Am. Chem. Soc.* **1993**, *115*, 1869.
(46) Shi, G.; Yu, B.; Xue, G.; Jin, S.; Li, C. *J. Chem. Soc., Chem. Commun.* **1994**, 2549.
(47) Onoda, M. *J. Appl. Phys.* **1995**, *78*, 1327.
(48) Rudge, A.; Raistrick, I.; Gottesfeld, S.; Ferraris, J. P. *Electrochim. Acta* **1994**, *39*, 273.
(49) Ferraris, J. P.; Henderson, C.; Torres, D.; Meeker, D. *Synth. Met.* **1995**, *72*, 147.
(50) Mastragostino, M.; Soddu, L. *Electrochim. Acta* **1990**, *35*, 463.
(51) Zagorska, M.; Krische, B. *Polymer* **1990**, *31*, 1379.
(52) Child, A. D.; Sankaran, B.; Larmat, F.; Reynolds, J. R. *Macromolecules* **1995**, *28*, 6571.
(53) Doblhofer, K.; Rajeshwar, K. In *Handbook of Conducting polymers* Skotheim, T., Eelsenbaumer, R. L., Reynolds, J. R., Ed.; Marcel Dekker: New York, Basel, Switzerland, and Hong Kong, 1998; p 557.
(54) Child, A. D.; Reynolds, J. R. *Macromolecules* **1994**, *27*, 1975.
(55) (a) Onoda, M.; Nakayama, H.; Morita, S.; Yoshino, K. *Synth. Met.* **1993**, *55*−*57*, 275. (b) Onoda, M.; Nakayama, H.; Morita, S.; Yoshino, K. *J. Appl. Phys.* **1993**, *73*, 2859.

MA992000T